RESEARCH PAPER

Build optimization of fiber-reinforced additively manufactured components

Aaditya Chandrasekhar[1] · Tej Kumar[1] · Krishnan Suresh[1]

Abstract

Additive manufacturing (AM) has enabled the fabrication of artifacts with unprecedented geometric and material complexity. The focus of this paper is on the build the optimization of short fiber reinforced polymers (SFRP) AM components. Specifically, we consider optimization of the build direction, topology, and fiber orientation of SFRP components. All three factors have a significant impact on the functional performance of the printed part. While significant progress has been made on optimizing these independently, the objective of this paper is to consider all three factors simultaneously and explore their interdependency, within the context of thermal applications. Towards this end, the underlying design parameters are identified, appropriate sensitivity equations are derived, and a formal optimization problem is posed as an extension to the popular Solid Isotropic Material with Penalization (SIMP). Results from several numerical experiments are presented, highlighting the impact of build direction, topology, and fiber orientation on the performance of SFRP components.

Keyword Build optimization · Fiber-reinforced · Topology optimization · Short fiber reinforced polymers

1 Introduction

Additive manufacturing (AM) has opened new opportunities to create parts with unprecedented geometric and material complexity. In AM, parts are fabricated layer by layer, as opposed to a subtractive process (Gibson et al. 2010). Fused deposition modeling (FDM) is one such AM process where a continuous thermoplastic (polymer) filament is deposited layer by layer (see Fig. 1a). With continuously improving materials and technology, FDM is being used today to make functional parts for thermal and structural applications. For example, Fig. 1b illustrates a heat exchanger where FDM's process capabilities are exploited to achieve large surface-to-volume ratio. Often, the structure can be optimized to reduce material consumption. Further, in such applications, to enhance performance, the polymer is often infused with short (typically, carbon) fibers (Botelho et al. 2003) (Fig. 1c). The functional properties of such short fiber–reinforced polymer (SFRP) components depend significantly on the fiber distribution and orientation. These can be controlled in FDM by suitability modifying the raster path.

The focus of this paper is on the build optimization of such SFRP components. Specifically, the objective is to optimize the build direction, the topology, and fiber orientation (raster path) for thermal applications. While significant progress has been made on each of these topics (for example, see Boschetto and Bottini (2014) and Fernandez-Vicente and Calle (2016)), the objective here is to consider all three factors simultaneously.

Towards this end, the remainder of this paper is organized as follows. The literature is reviewed with a motivating example in Section 2, and research gaps are identified. This is followed by a discussion on problem formulation and derivation of sensitivity equations in Section 3. Results are discussed in Section 4, with a concluding note in Section 6.
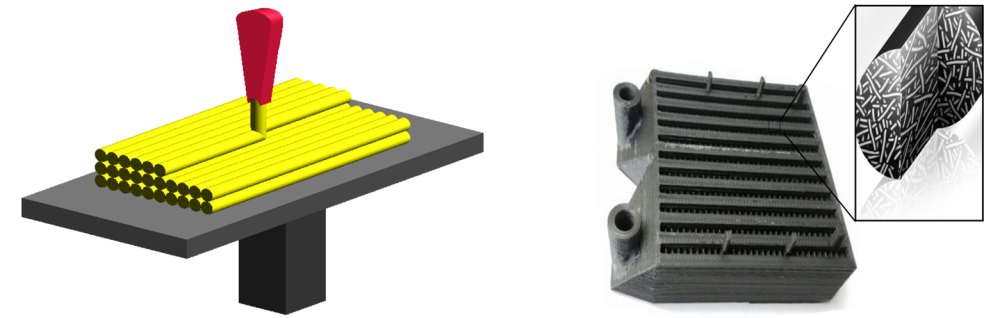
✉ Aaditya Chandrasekhar
   achandrasek3@wisc.edu

   Tej Kumar
   tkumar3@wisc.edu

   Krishnan Suresh
   ksuresh@wisc.edu

[1]   Department of Mechanical Engineering, University
      of Wisconsin-Madison, Madison, WI 53706, USA

Fig. 1 Fused deposition modeling of fiber-filled composites

(a) Illustration of the fused deposition modeling [45].

(b) A heat exchanger is printed using Carbon fiber reinforcement. This illustrates some of the recent advances in AM to print functional components. The image portrays the infill strategy used and the presence of fiber reinforcement in the polymer matrix.
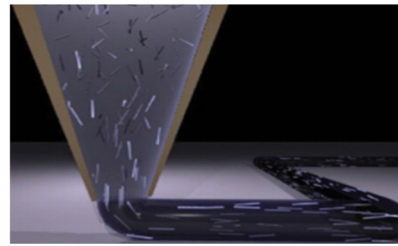
(c) Polymers are filled with fibers to enhance mechanical properties [53]

2 Literature review

As discussed in the previous section, the objective here is to simultaneously optimize the *build direction*, the *topology*, and *fiber orientation*, to improve functional performance of SFRP parts. Prior work related to the above three build parameters is discussed next.

2.1 Build direction

The build direction plays a significant role in the surface quality, print time, and sacrificial support of FDM components (see (Boschetto and Bottini 2014; Das et al. 2015; Qian 2017; Mohamed et al. 2015; Sanati Nezhad et al. 2010; Zhang et al. 2015). While these are important metrics, the current work focuses on the interplay between build direction and functional performance of the part. Specifically, it is well known that FDM introduces behavioral anisotropy (Mirzendehdel et al. 2018), primarily due to incomplete fusion between adjoint layers. For example, consider Fig. 2a where a heat load is applied on the top surface, and the temperature is fixed at the bottom. Figures 2b and c illustrate two possible build directions. Observe that, in the former, the interlayer resistance is in the direction of heat flow and is therefore not preferable, i.e., the build direction along X (or Y in this example) is preferable from a performance perspective. This simple example illustrates the importance of build direction on part performance. However, the optimal build orientation might not be obvious in many cases (see numerical examples).
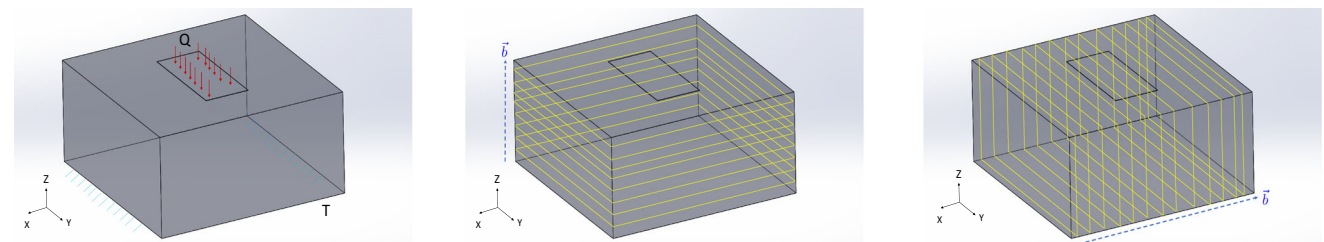
(a) A domain with thermal boundary conditions.

(b) Build direction along Z increases thermal resistance.

(c) Build direction along X reduces thermal resistance.

Fig. 2 Build orientation for optimizing functional performance of FDM

Researchers have proposed methods to optimize build direction for part performance. For example, Umetani and Schmidt (2013) proposed a structural analysis technique based on a bending moment concept to optimize the build direction; however, isotropic material was assumed for simplicity, i.e., fiber reinforcement was not considered. On the other hand, material anisotropy was considered by Erva (Ulu et al. 2015) where the build direction was optimized to maximize structural safety factor using a surrogate-optimization model.

2.2 Topology

With the advent of AM, there has been significant interest in optimizing the topology to improve part performance. For the above example, with X-axis as the build direction, Fig. 3 illustrates an optimal topology of 50% mass, compared with the original design, with minimal loss in performance. Various techniques such as Solid Isotropic Material with Penalization (SIMP) (Gersborg-Hansen et al. 2006; Bendsoe and Sigmund 2003; Sigmund 2001), level-set (Wang et al. 2003), Evolutionary Structural Optimization (ESO) (Xie and Steven 1993), and topological-sensitivity (Suresh 2010) may be employed for topology optimization. The limitation of prior work is that they assume a pre-defined build direction and typically disregard material anisotropy (see Mirzendehdel et al. (2018) for exception).

Instead of optimizing the topology, researchers have also considered optimizing infill patterns. Martínez et al. (2016) proposed a stochastic method to generate compliant structures with a voronoi infill. Recently, Chougrani et al.

(2017) suggested a lattice infill for AM. Wu et al. proposed a two-scale simultaneous optimization of shell-infill in the context of minimizing structural compliance (Jun et al. 2017). Manufacturability of the model has been paid considerable consideration in works such as in Jun et al. (2016) and Qian (2017) . Various attempts have been made to link micro-scale infill topology to the density values obtained through optimization. *Multi-scale* optimization has been addressed in Yan et al. (2016), Sivapuram et al. (2016), and Yi et al. (2012). Recently, Dapogny et al. (2019) performed a 2D topology optimization considering specific infill patterns with anisotropic behavior.

The focus of this paper is on optimizing the topology, as opposed to finding an optimal infill pattern.

2.3 Fiber orientation/print strategy

Finally, the print strategy can also have a significant impact on part performance, especially in the case of fiber reinforced polymers (Blok et al. 2018), since (1) fibers preferentially orient in the direction of extrusion of the filament from the print nozzle (Brenken et al. 2018) and (2) fibers add additional strength and thermal conductivity to the material (Liu et al. 2018). Thus, an optimized fiber orientation/print pattern as in Fig. 4 can improve part performance. Towards this end, Raney et al. (2018) recently introduced methods of achieving local site-specific control of fiber orientation. This coupled with development in multi-axis printing (Dai et al. 2018) paves new avenues to realize functionally tailored components with in-situ control of fiber composites. The problem of optimizing fiber orientation angle has been addressed within the context of laminar composites. Discrete material optimization (DMO) is one of the most popular approaches, where a list of a priori directions (e.g., $0°$, $±45°$, $±90°$) (Stegmann and Lund 2005) is used. This avoids local minima but can result in sub-optimal results. Interpolation schemes have also been suggested to overcome this limitation. Alternately,
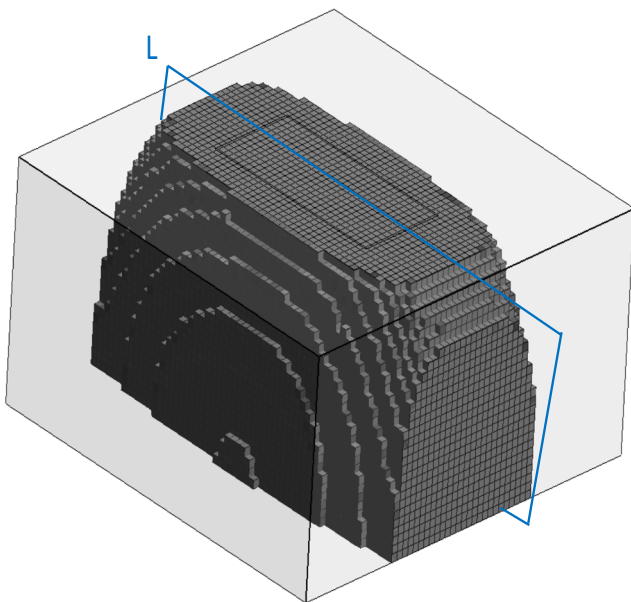

Fig. 3 The design shown in Fig. 2a is optimized to 50 % of its initial volume
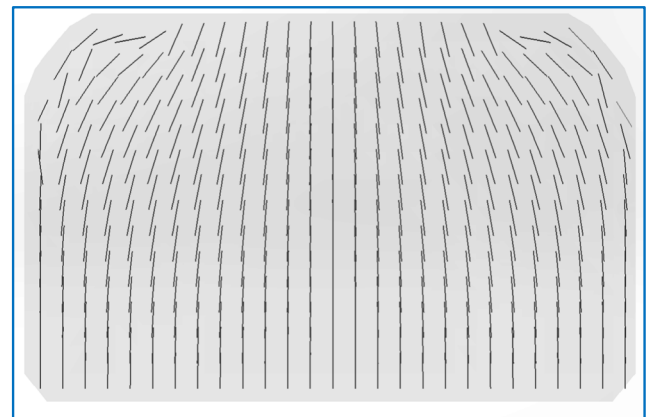

Fig. 4 Optimizing the print strategy can improve part performance

continuous fiber angle optimization (CFAO) has also been proposed (Brampton et al. 2015). This offers greater design freedom but can result in local minima. While the focus has been on laminar composites, there has been a recent increase in targeting these methodologies for AM. More references can be found at Walker and Smith (2003), Luo and Gea (1998), Bendsoe et al. (2008), Huang and Haftka (2005), Gürdal et al. (1999), and Pedersen (1989).

2.4 Paper contributions

The main contribution of this paper is a *comprehensive* approach to the build optimization of thermally loaded SFRP components by simultaneously considering the impact of build direction, print topology, and fiber orientation. In particular, the proposed formulation is an extension to the popular SIMP method (Sigmund 2001).

3 Problem formulation

We start by discussing the design variables used in our formulation. This leads to a discussion on the optimization problem, sensitivity analysis, and proposed algorithm.

3.1 Design parameters

3.1.1 Build direction

Due to the incomplete fusion between subsequent layers of deposited material, the thermal conductivity tends to be lower in the direction of the build, leading to transversely isotropic properties. Prajapati et al. (2018) proposed to model the effective thermal conductivity along the build direction via

$$\frac{1}{k_z} = \frac{w_a + w_f}{w_a k_a + w_f k_f} + \frac{R_c}{L_h} \tag{1}$$

where k_z is the thermal conductivity in the build direction, k_a is the thermal conductivity of air, k_f is the thermal conductivity of the filament (with no fiber reinforcement), w_a is the air gap between rasters, and w_f is the width of the raster. R_c is the contact resistance between adjacent layers, and L_h is the layer height. This is illustrated in Fig. 5. Experimental studies show R_c to be in the order of $500 - 2000$ $[\mu K m^2 W^{-1}]$ leading to $k_z/k_f \approx 0.6 - 0.8$. Similar decrease in mechanical properties has been reported by Knoop and Schoeppner (2015) and Farzadi et al. (2014). Observe that the build-direction anisotropy is different from fiber-induced anisotropy (Zhang et al. 2017).

In our formulation, we assume the part to have an initial build direction along the global Z-axis. We introduce *two* design parameters α_0 and β_0 as Eulerian angles to capture the rotation of the build direction about the global X- and Y-axis respectively via (2). These two angle parameters are to be determined by the optimizers.

$$\mathbf{b} = R_x(\alpha_0) R_y(\beta_0) \mathbf{z} \tag{2}$$

where R_x and R_y are standard rotation matrices.

Fig. 5 Illustration showing thermal conductivity of a printed component
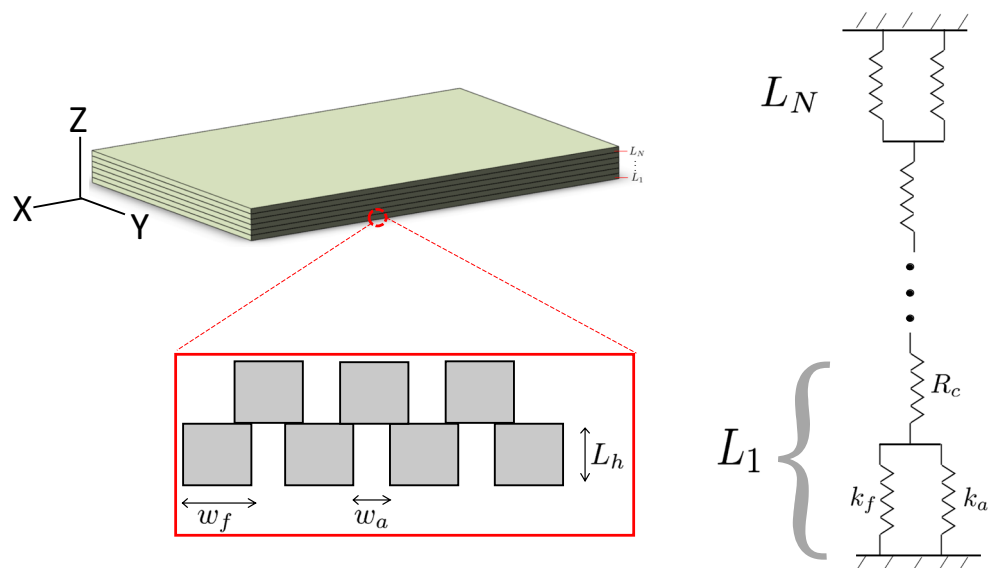
3.1.2 Topology

Next, we consider the parameterization of topology. Here, the evolution of the topology is modeled using classic SIMP where each finite element e is assigned a density value $\rho_e \in [0, 1]$. A density value of one denotes the presence of material, and zero its absence. The density is further penalized by a constant p relating the material property via a power-law:

$$[K]_e = [K_0] + \rho_e^p([\hat{K}] - [K_0]) \tag{3}$$

where $p = 3$, and $[k_0]$ is a small thermal conductivity assigned to void elements to prevent singularities.

3.1.3 Fiber orientation

Next, we consider anisotropy due to fiber orientation. Mulholland et al. (2016) reported thermal anisotropy of specific SFRP materials (see Table 1). For example, the baseline conductivity was reported to be $0.26[W/m - K]$ for *PA6-CuF-20*, significantly lesser than the fiber-infused counterpart. Here, $k_\parallel$ is the thermal conductivity achieved along the principal direction of the fibers, leveraging their higher conductivity and $k_\perp$ can be attributed as the thermal conductivity imparted by the filament matrix. Since $k_\perp/k_\parallel \approx 0.13 - 0.38$, it is important to orient the fibers in an optimal fashion.

The finite element formulation used here (see later section) utilizes a geometrically congruent hexahedral (voxel) mesh. Thus, every finite element e is assigned an orientation angle of θ_e, on a plane perpendicular to the build direction. This angle will be determined by the optimizer, and the resulting conductivity matrix can be expressed as:

$$[K]_e = R_{\mathbf{b}}(\theta_e)\hat{K} R_{\mathbf{b}}^T(\theta_e) \tag{4}$$

$$[\hat{K}] = \begin{bmatrix} k_\parallel & 0 & 0 \\ 0 & k_\perp & 0 \\ 0 & 0 & k_z \end{bmatrix} \tag{5}$$

where $[\hat{K}]$ is the thermal conductivity matrix along the principal directions assumed to be coincident with the global coordinates of the model. Combining the anisotropy due to layer-wise build (as discussed in the previous section) with that imparted by the fibers, we can see that $k_z/k_\perp \approx 0.08 - 0.31$. Further, $[R_{\mathbf{b}}(\theta_e)]$ expresses the orientation of the infill fiber material with respect to the build direction.

3.1.4 Summary

Piecing all the design variables together, we have the effective conductivity given by:

$$[K]_e = [K_0] + \rho_e^p(R(\alpha_0, \beta_0, \theta_e)([\hat{K}] - [K_0])R(\alpha_0, \beta_0, \theta_e)^T) \tag{6}$$

where the rotation matrix is given by:

$$R(\alpha_0, \beta_0, \theta_e) = \begin{bmatrix} 1 & 0 & 0 \\ 0 & \cos(\alpha_0) & -\sin(\alpha_0) \\ 0 & \sin(\alpha_0) & \cos(\alpha_0) \end{bmatrix} \begin{bmatrix} \cos(\beta_0) & 0 & \sin(\beta_0) \\ 0 & 1 & 0 \\ -\sin(\beta_0) & 0 & \cos(\beta_0) \end{bmatrix} \begin{bmatrix} \cos(\theta_e) & -\sin(\theta_e) & 0 \\ \sin(\theta_e) & \cos(\theta_e) & 0 \\ 0 & 0 & 1 \end{bmatrix} \tag{7}$$

Observe that (6) combines the effect of build direction (α_0 and β_0), fiber orientation (θ_e), and infill density (ρ_e), resulting in $2n+2$ degrees of freedom where n is the number of finite elements.

3.2 Optimization formulation

We are now ready to formulate the optimization problem. For a typical thermal problem, our objective is to minimize thermal compliance (see Gersborg-Hansen et al. 2006; Gao et al. 2008; Li et al. 1999; Deng and Suresh 2015), subject to a volume constraint:

$$\min_{\Omega \subset \Omega_0} \quad C = \int_\Omega f\Theta d\Omega = \{f\}^T\{\Theta\} \tag{8}$$

$$\text{s.t.} \quad g(\rho) = \frac{\int_\Omega \rho d\Omega}{V^*} - 1 \leq 0 \tag{9}$$

$$[K]\{\Theta\} = \{f\} \tag{10}$$

$$\alpha_0 \in [0, 2\pi] \tag{11}$$

Table 1 Thermal conductivity of a few SFRPs

Material	$k_\parallel[W/(m - K)]$	$k_\perp[W/(m - K)]$
Onyx	0.88	0.30
PA6-CuF-20	4.84	0.76
PA6-CuF-25	5.52	0.77
RTP 0299 X 137152 C NAT/BLK	5.00	1.50
RTP 0299 X 137077 C NAT/BLK	18.01	4.50

$$\beta_0 \in [0, \pi] \tag{12}$$

$$\theta_e \in [0, 2\pi] \quad \forall e \tag{13}$$

$$\rho_e \in [0, 1] \quad \forall e \tag{14}$$

Observe that the system is governed by linear equations (10) derived from the finite element discretization of a steady state heat conduction problem. $[K]$ is the stiffness matrix, $\{\Theta\}$ is the temperature field, and $\{f\}$ is the external heat applied. V^* in (9) refers to the final volume to be achieved upon optimization. The optimizer used here is the GCMMA (Svanberg 1987); this requires that the design variables be bounded. Thus, thoughthe angular variables (namely α_0, β_0, and θ_e) are periodic, and no bounds are required, limits are imposed as shown. The constraints for the build orientation is given by (11) and (12). The constraint for fiber orientation is given by (13), and (14) sets the limit for density.

3.3 Sensitivity analysis

In order to perform gradient-based optimization, the sensitivity of the objective and constraints, with respect to the design variables is derived in this section.

3.3.1 Objective sensitivity

Recall that the thermal compliance is given by:

$$\mathcal{C} = \{f\}^T\{\Theta\} \equiv \{\Theta\}^T[K]\{\Theta\} \tag{15}$$

Differentiating (15) with respect to a generic design variable x_i, we have

$$\frac{\partial\{\mathcal{C}\}}{\partial x_i} = \frac{\partial\{\Theta\}}{\partial x_i}^T[K]\{\Theta\} + \{\Theta\}^T\frac{\partial[K]}{\partial x_i}\{\Theta\} + \{\Theta\}^T[K]\frac{\partial\{\Theta\}}{\partial x_i} \tag{16}$$

Neglecting design-dependent loads, we have $\frac{\partial f}{\partial x_i} = \mathbf{0}$, (10) is differentiated with respect to design variable x_i to get

$$\frac{\partial\{\Theta\}}{\partial x_i} = -[K]^{-1}\frac{\partial[K]}{\partial x_i}\{\Theta\} \tag{17}$$

Inserting (17) into (16) results in:

$$\frac{\partial\{\mathcal{C}\}}{\partial x_i} = -\{\Theta\}^T\frac{\partial[K]}{\partial x_i}\{\Theta\} \tag{18}$$

In particular, we have

$$\frac{\partial[K]}{\partial\rho_e} = \iiint_{\Omega_e}[B]^T\frac{\partial[k]_e}{\partial\rho_e}[B]d\Omega_e \tag{19}$$

where $[B]$ is the gradient of the shape function matrix and

$$\frac{\partial[k]_e}{\partial\rho_e} = p\rho_e^{p-1}([R(\alpha_0,\beta_0,\theta_e)]([\hat{k}]-[k_0])[R(\alpha_0,\beta_0,\theta_e)]^T) \tag{20}$$

Similarly, the sensitivity with respect to θ_e is given by:

$$\frac{\partial[K]}{\partial\theta_e} = \iiint_{\Omega_e}[B]^T\frac{\partial[k]_e}{\partial\theta_e}[B]d\Omega_e \tag{21}$$

where

$$\frac{\partial[k]_e}{\partial\theta_e} = \rho_e^p\left(\frac{\partial[R(\alpha_0,\beta_0,\theta_e)]}{\partial\theta_e}([\hat{k}]-[k_0])[R(\alpha_0,\beta_0,\theta_e)]^T\right.$$
$$\left. + [R(\alpha_0,\beta_0,\theta_e)]([\hat{k}]-[k_0])\frac{\partial[R(\alpha_0,\beta_0,\theta_e)]^T}{\partial\theta_e}\right) \tag{22}$$

The sensitivity with respect to build orientation angle α_0 is given by

$$\frac{\partial[K]}{\partial\alpha_0} = \sum_e \iiint_{\Omega_e}[B]^T\frac{\partial[k]_e}{\partial\alpha_0}[B]d\Omega_e \tag{23}$$

where $\frac{\partial[k]_e}{\partial\alpha_0}$ follows an expression similar to that of (22). The sensitivity with β_0 follows suit with α_0 and is omitted here for sake of brevity. Further, we note the highly coupled nature of the different design variables and the interplay between density, fiber directions, and build orientation in determining the objective and sensitivities, thus strengthening the argument for the need of a coupled solver.

Note that the sensitivity with respect to the build orientation angles (23) is summed over all elements. This is in contrast to sensitivity with respect to infill densities (20) and fiber orientation (21). In other words, build orientation is global, while infill density and fiber orientation apply to each element.

3.3.2 Constraint sensitivity

The global volume constraint (9) in the discrete form can be expressed as

$$\frac{\sum_e \rho_e v_e}{V^*} - 1 \leq 0 \tag{24}$$

where v_e is the volume of a discrete element in the congruent hexahedral voxel mesh. The gradient of the global volume constraint with density can be obtained as,

$$\frac{\partial g}{\partial\rho_e} = \frac{v_e}{V^*} \tag{25}$$

The sensitivity is zero with respect to θ_e, α_0, and β_0. The box constraints limiting the range of the design variables given by (11), (12), (13), and (14) are considered implicitly by the globally convergent method of moving asymptotes (GCMMA) solver used in this paper (Svanberg 1987). While any finite element solver can be used, an in-house assembly-free solver (Mirzendehdel and Suresh 2015; Yadav and Suresh 2014) is employed here.

3.4 Optimization algorithm

The optimization algorithm utilizes GCMMA (Svanberg 1987) to optimize and an in-house assembly free finite element solver to perform the FEA (Yadav and Suresh 2013). The algorithm followed is described below (algorithm 1):

Algorithm 1 Build, infill and fiber optimization.

1: **procedure** BUILDOPT(V_c)   ▷ Max. Vol. Frac.
   $V_c \in [0, 1]$
2:     $i = 0$ ▷ Iteration Index
3:     $\phi = \{\bar{\rho}, \bar{\theta}, \alpha_0, \beta_0\}$ ▷ Opt. Variables
4:     $\Delta = 1.0$ ▷ Design Change
5:     **while** $\Delta > \epsilon$ and $i \leq$ MaxIter **do**
6:         $i \leftarrow i + 1$
7:         $[K] \leftarrow (\phi)$ ▷ via (6)
8:         $\{\Theta\} \leftarrow [K]^{-1}\{f\}$ ▷ Deflated-Preconditioned
   Assembly-Free solver
9:         $\mathcal{C} \leftarrow (\{\Theta\}, \{f\})$ ▷ via (15)
10:        $g \leftarrow (\bar{\rho}, V^*)$ ▷ Vol. Constraint (24)
11:        $(\frac{\partial \mathcal{C}}{\partial \rho_e}, \frac{\partial \mathcal{C}}{\partial \theta_e}, \frac{\partial \mathcal{C}}{\partial \alpha_0}, \frac{\partial \mathcal{C}}{\partial \beta_0}, \frac{\partial g}{\partial \rho_e})$ ▷ via (20), (22), (23),
   (25)
12:        $\phi^i \leftarrow (\mathcal{C}, g, \frac{\partial \mathcal{C}}{\partial \rho_e}, \frac{\partial \mathcal{C}}{\partial \theta_e}, \frac{\partial \mathcal{C}}{\partial \alpha_0}, \frac{\partial \mathcal{C}}{\partial \beta_0}, \frac{\partial g}{\partial \rho_e})$ ▷
   GCMMA Solver (Svanberg 1987)
13:        $\Delta = (|\phi_e^i - \phi_e^{i-1}|)$

4 Numerical experiments

We now demonstrate the proposed method through several examples. The examples considered and the corresponding sub-sections are summarized in Table 2. For example, in Section 4.1.1, we optimize just the topology, by assuming a fixed build direction and fixed fiber orientation. Similarly, in Section 4.1.2, we optimize just the fiber orientation, by assuming a fixed build direction, fixed fiber orientation, topology, and so on. The examples were chosen to highlight the importance of one or more design variables. All experiments were conducted on a desktop PC equipped with an Intel i7 12-core processor with 32 GB RAM running at 3.2 GHz.

Table 2 Summary of various examples considered

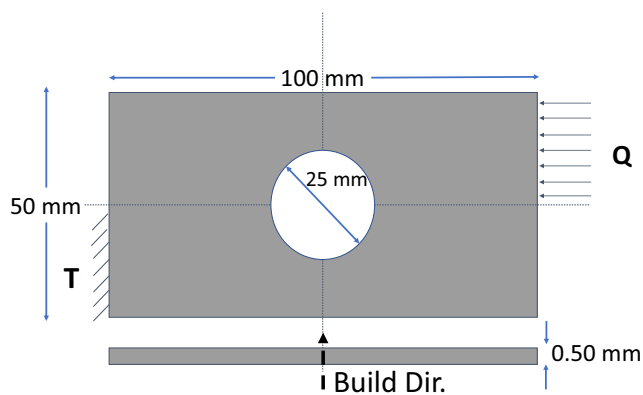| Section	Build Dir	Fiber Orient.	Topology
4.1.1	×	×	✓
4.1.2	×	✓	×
4.1.3	×	✓	✓
4.2, 4.3	✓	×	✓
4.4	✓	✓	✓

Fig. 6 Illustration of a plate problem with thermal boundary conditions

4.1 Fixed build orientation

In this section, the build orientation is assumed to be fixed, while the topology and/or the fiber orientation are optimized.

4.1.1 Optimization of topology

Consider a plate, with a thickness of 0.5 mm, illustrated in Fig. 6. The thermal boundary conditions are applied as illustrated in Fig. 6, where $T = 0°C$ and the heat flux $Q = 10^4 [W/m^2]$. The build direction is along the thickness direction. Further, in this subsection, the material is assumed to be isotropic with $k = 0.77$ [W/m-K], and therefore, the fiber orientation is not relevant. The only design variables are the SIMP densities; the thermal compliance must be minimized for a target volume fraction of 0.5. For finite element analysis, the domain is discretized into 25,000 hexahedral elements (voxels).

To optimize the topology, all elements are assigned an initial density of 0.5 (the target volume fraction). The optimization algorithm described earlier is now exploited to find the optimal topology that minimizes the thermal compliance. The optimization terminates when the relative
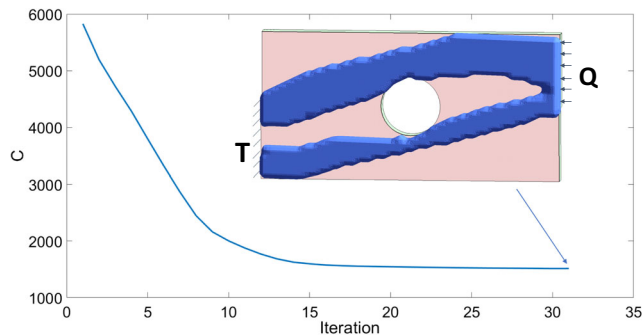

Fig. 7 Topology and convergence plot for plate problem

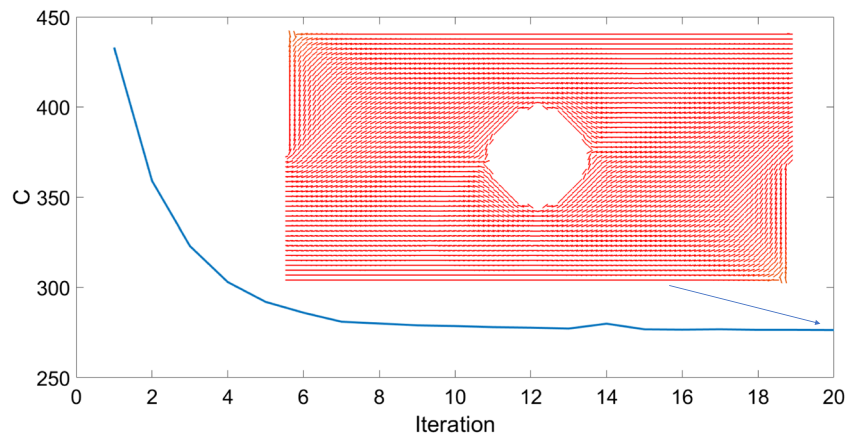**Fig. 8** Fiber orientation and convergence plot for plate problem

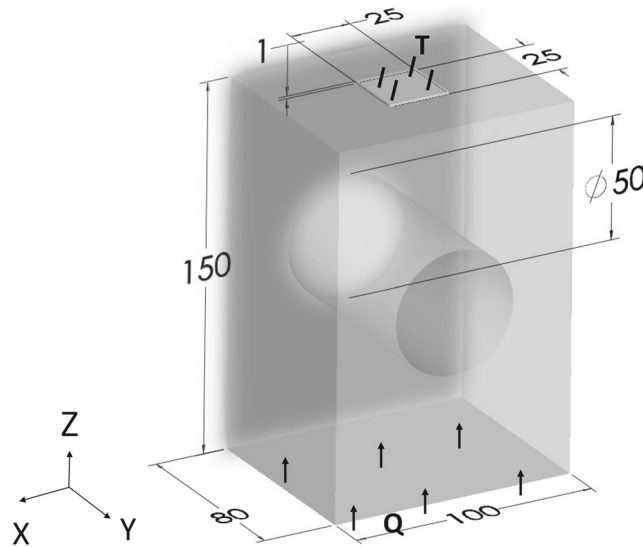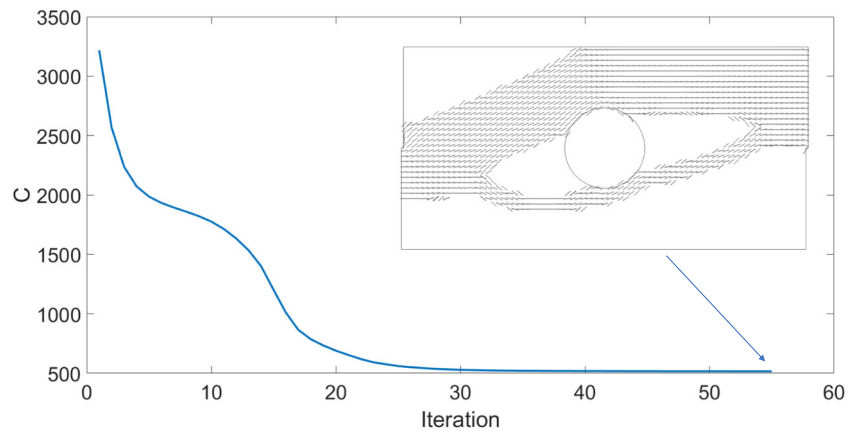**Fig. 9** Fiber orientation and convergence plot for 2D plate problem

Fig. 10 A box geometry with a center hole and associated boundary conditions. All dimensions in mm

Table 3 Compliances and computational time with and without build direction optimization

Volume fraction (%)	Fixed build Dir. $\mathbf{b} = \{0, 0, 1\}$		Optimized build Dir.		
30	C = 13.2	t= 12.2 mins	C = 4.54	$\mathbf{b} = \{0.93, 0.27, 0.24\}$	t = 18.1 mins
50	C = 4.33	t = 9.1 mins	C = 1.56	$\mathbf{b} = \{0.97, 0.21, 0.12\}$	t = 14.3 mins
75	C = 2.42	t = 6.7 mins	C = 1.00	$\mathbf{b} = \{0.96, 0.24, 0.14\}$	t = 11.2 mins

Fig. 11 Topologies at 30% volume fraction for fixed and optimized build orientation

(a) Result with fixed build orientation.

(b) Result with optimized build orientation.
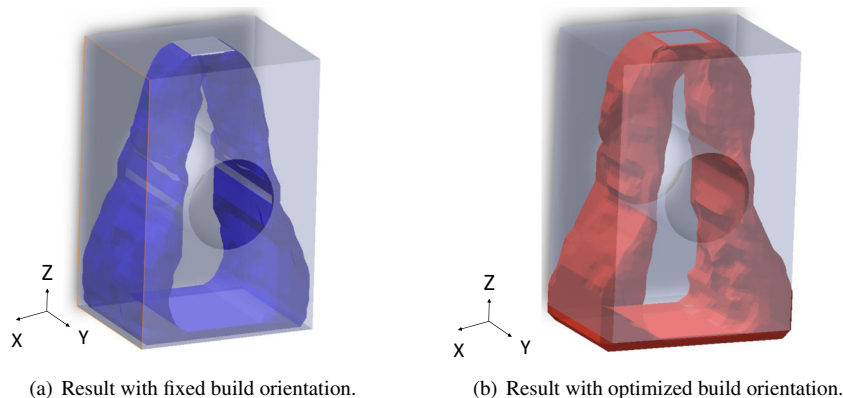
change in the thermal compliance is less than 10^{-4}. The final topology, together with the convergence, is illustrated in Fig. 7; observe that the topology aligns with the flow of heat, as expected. The solver completed the optimization in 27 iterations, taking a total time of 3.27 min.

4.1.2 Fiber optimization

Next, we consider optimizing just the fiber orientation for the above example; the build direction is fixed as before, and the topology is not optimized, i.e., 100% volume. The material is assumed to be *PA6-CuF-25* (see Table 1); the anisotropic conductivity is an impetus for preferential fiber orientation. All elements are initially oriented with $\theta_e = 0°$. After optimization, Fig. 8 illustrates convergence and the orientation of the fibers. The solver completed the optimization in 20 iterations, taking a total time of 2.81 min.

4.1.3 Fiber and topology optimization

Next, we combine fiber and topology optimization for the above example. All elements have an initial density of 0.5, and the fibers are oriented at $\theta = 0°$. Figure 9 illustrates the convergence and the resulting topology, with fiber orientation. We observe a significant improvement in performance, compared with only optimizing the topology (Section 4.1.1) or the fibers (Section 4.1.2). The solver completed the optimization in 50 iterations, taking a total time of 4.15 min.

4.2 Build orientation and topology optimization

We now illustrate an example where the benefits of optimizing the build direction become evident. Consider the geometry in Fig. 10, where $T = 0°C$ on the (a subset of the) top face and a heat flux of 10^3 W/m^2 is applied on the bottom face. The material is assumed to be isotropic, i.e., fiber orientation is disregarded. However, observe that

depending on the build direction, inter-layer anisotropy will be induced. For example, if the build direction is along Z-axis, then $k_x = k_y = 0.76$ [W/m-K] while $k_z = 0.45$ [W/m-K]. For finite element analysis, the domain was meshed with 100,000 elements.

To isolate the impact of build direction, two sets of optimization studies were carried out. In the first set, the build direction was fixed along Z-axis; observe that this is sub-optimal since the heat sink and source are separated along the Z-axis. The topology was then optimized for 3 different volume fractions: 30%, 50%, and 75%. The final compliances and time taken are reported in the second column of Table 3. In the second set, the build direction was also optimized (with an initial guess along Z-axis). The thermal compliance, together with the optimal build direction and time taken are reported in the third column; the optimal build direction is approximately along X-axis. As one can observe, the compliance reduces significantly when the build direction is optimized. The final topologies at 30% volume fraction from the two sets are shown in Fig. 11.
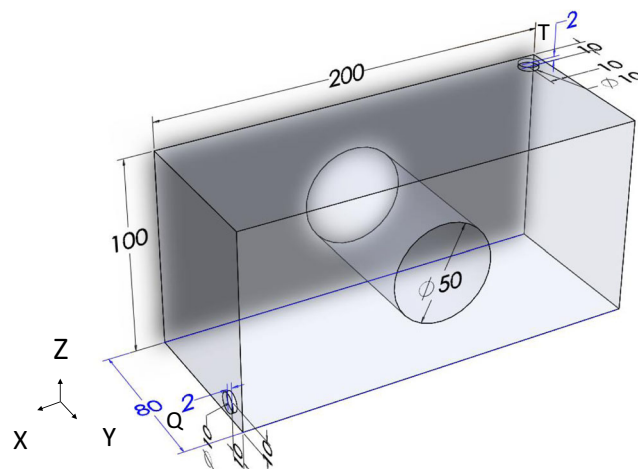

Fig. 12 Geometry and boundary conditions to compare sequential and simultaneous optimization

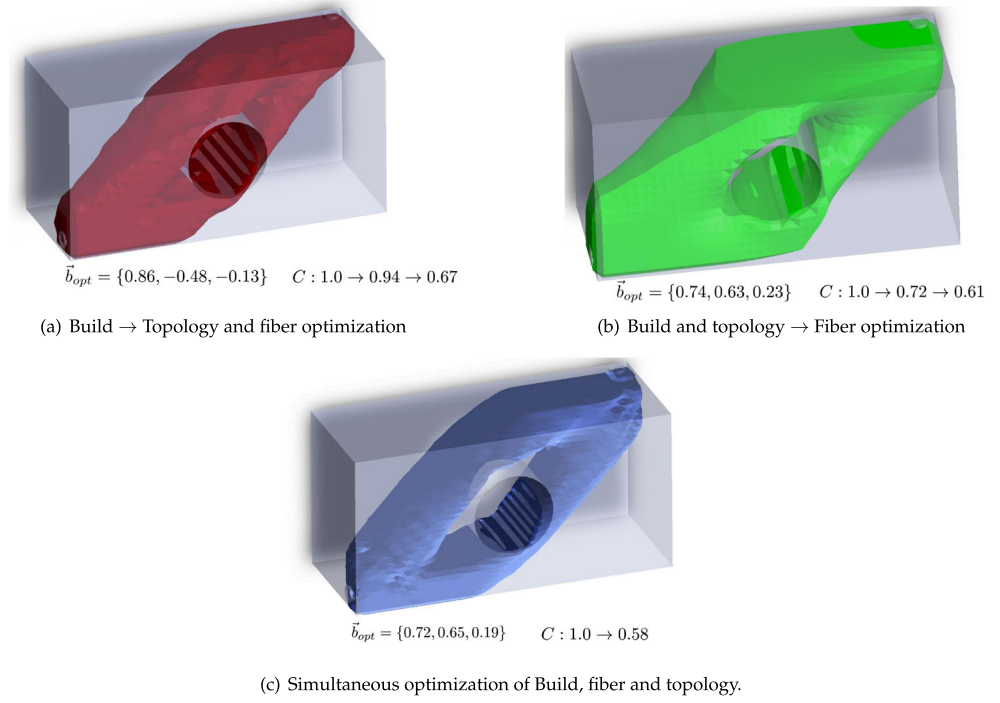**Fig. 13** Comparison of sequential and simultaneous optimization

$\vec{b}_{opt} = \{0.86, -0.48, -0.13\}$ $C : 1.0 \to 0.94 \to 0.67$

(a) Build → Topology and fiber optimization

$\vec{b}_{opt} = \{0.74, 0.63, 0.23\}$ $C : 1.0 \to 0.72 \to 0.61$

(b) Build and topology → Fiber optimization

$\vec{b}_{opt} = \{0.72, 0.65, 0.19\}$ $C : 1.0 \to 0.58$

(c) Simultaneous optimization of Build, fiber and topology.
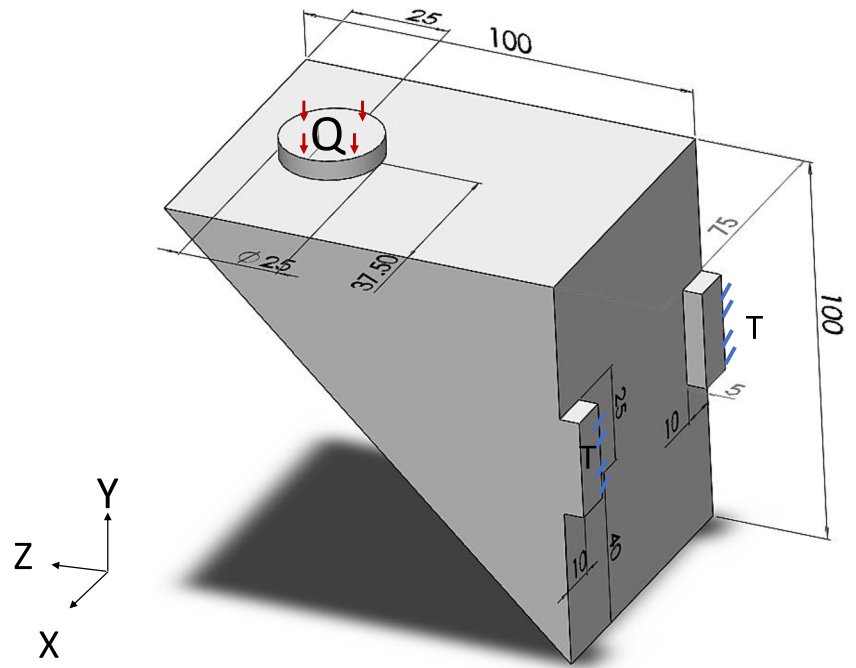
Fig. 14 A triangular block with boundary conditions

Table 4 Impact of initial build direction on the optimal build direction and compliance

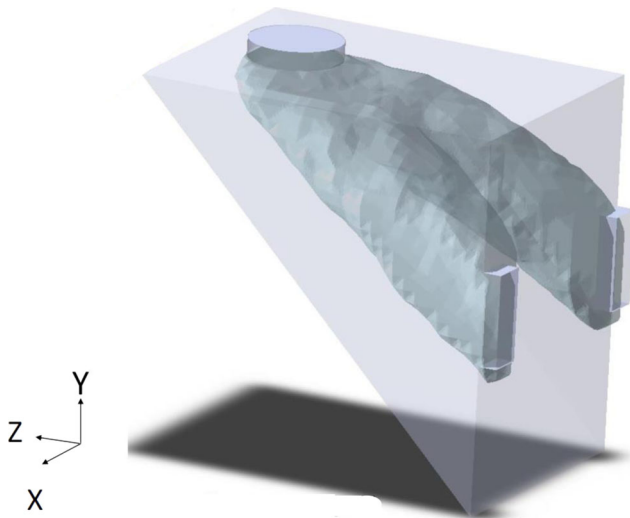| Trial	$\mathbf{b}_{init}$	$\mathbf{b}_f$	C_0	C_f
1	$\{1, 0, 0\}$	$\{0.773, 0.63, 0.006\}$	19813	803
2	$\{0, 1, 0\}$	$\{-0.773, -0.634, -0.0019\}$	38059	823
3	$\{0, 0, 1\}$	$\{-0.776, 0.63, 0.002\}$	43945	858
4	$\{1/\sqrt{2}, -0.5, 0.5\}$	$\{0.773, -0.63, 0.0037\}$	22491	873

Fig. 15 The final topology and build direction upon optimization

4.3 Sequential vs. simultaneous optimization

In this example, we illustrate the strong interplay between the three sets of design parameters. Consider the geometry and thermal boundary conditions illustrated in Fig. 12, with $Q = 10,000 [W/m^2]$ and $T = 0°C$. As before, we set $k_\parallel = k_\perp = 0.76 [W/m - K]$ and $k_z = 0.45 [W/m - K]$. The domain was meshed with 10,000 elements, and the target volume fraction was 0.5. We consider here three optimization scenarios. In the first scenario, we first optimize the build orientation (for full volume), and then optimize the topology and fiber orientation, using the computed build direction. In the second scenario, the build direction and topology are optimized simultaneously, following which the fiber orientation is optimized. Finally,
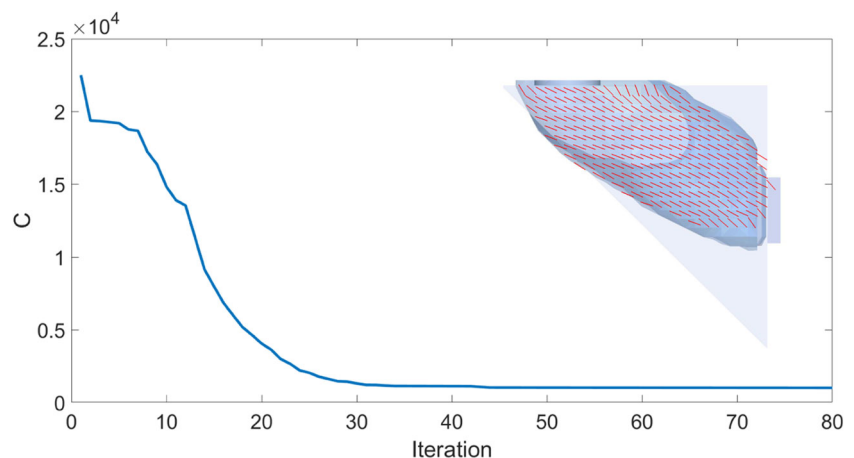
in the third scenario, all three (build, topology, and fiber orientation) are simultaneously optimized.

The resulting designs are presented in Fig. 13a–c respectively. The topologies exhibit minor differences, but the optimal build directions are significantly different. Further, in the first scenario, the relative compliance dropped to 0.94 (after optimizing just the build direction taking 23 CG iterations), and then to 0.67 (after optimizing the topology and fiber with 62 CG Iterations), taking a total of 85 CG iterations. In the second scenario, the relative compliance dropped to 0.72 (showcasing the effect of build and topology) which then reduced to 0.61 after 41 and 37 CG iterations respectively, totaling to 78 iterations. Finally, optimizing all three variables simultaneously results in the lowest compliance of 0.58 after 91 CG iterations. Comparing the final compliance of 13 a and c, we note that the combined optimization consumes about 16% more iterations for about 6% gain in performance. This can be attributed to the oscillatory behavior in the convergence of the optimizer and the subjective nature of the problem.

4.4 Complete optimization

In this section, we highlight the full potential of the solver by simultaneously optimizing the build direction, topology, and fiber orientation, for the geometry in Fig. 14. The prescribed boundary conditions are a fixed temperature of $0°C$ and a heat flux of 10^4 [W/m^2]. We assume the material be *PA6-CuF-25* (Table 1) with $k_z = 0.45$ [W/m-K]. The desired volume fraction is 0.3. The design is discretized with 50,000 elements. As before, the initial density of all the elements is 0.3 (desired volume fraction), the orientation of the fibers is 0°. Several instances of optimization were executed using different initial build orientation; the results are tabulated in Table 4. While the final build direction is almost identical in each case (upto a sign), the final compliances are slightly different.

Fig. 16 The evolution of compliance with iteration. The final topology along with orientation of the fiber at a cross section is shown

Fig. 17 The convergence of the norm of the difference between the optimal build vector and that at given iteration
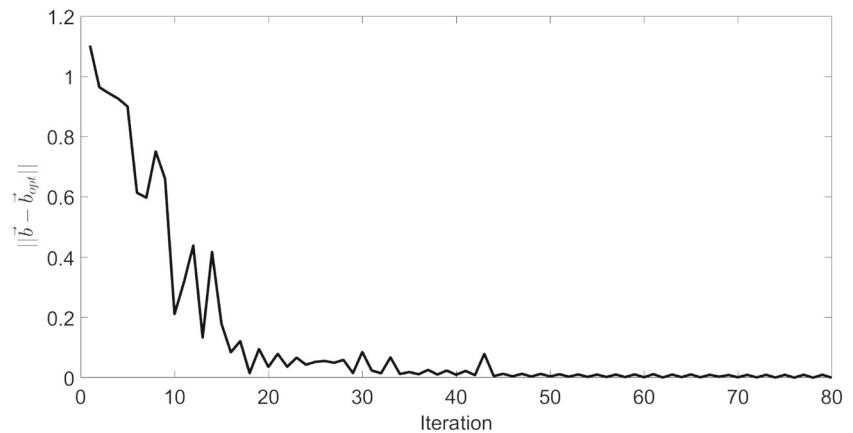
This reflects the sensitivity of the compliance to the build direction.

The optimal topology and build direction are illustrated in Fig. 15.

The compliance convergence (for the fourth build orientation scenario) is plotted in Fig. 16, together with the optimal fiber orientation for one of the cross sections. We observe a sharp decrease in the compliance near the 20th iteration; this can be attributed to the convergence in the build orientation.

The convergence of the build direction is illustrated in Fig. 17. We observe that the optimizer considers various orientations to finally arrive at the optimal. Further, we notice that the convergence of the orientation is non-smooth. We conjecture that the oscillatory nature is due to the strong interplay between the build orientation and the evolving topology/ fiber orientation. The solver completed the optimization in 80 iterations taking a total time of 38.5 min.

5 Conclusion

The main contribution of this paper is an integrated framework for the simultaneous optimization of build direction, topology, and fiber orientation of SFRP components. The numerical experiments demonstrated that all three factors must be considered for optimal performance. A global volume constraint was imposed to drive the optimizer towards minimizing compliance. The layer-wise printing paradigm of AM was of central focus, and methods were proposed to include the consequence of anisotropic material properties.

There are several areas for future research. The present formulation does not include several AM-constraints such as overhang surfaces, minimum feature size, and surface finish. Further post-processing (Allaire et al. 2018) might be required to produce smooth transitions in fiber orientation. Generation of machine instructions from the obtained topology and orientation field is also a topic of future research (Steuben et al. 2016).

6 Replication of results

The paper uses the Pareto code, developed at UW-Madison, that has been assigned to the Wisconsin Alumni Research Foundation (WARF). Due to restrictions imposed by WARF, we are unable to provide public access to this software for replication of results.

Compliance with Ethical Standards

Conflict of interest The authors declare that they have no conflict of interest.

Disclaimer The views and opinions of authors expressed herein do not necessarily state or reflect those of the United States Government or any agency thereof. Prof. Suresh is a consulting Chief Scientific Officer of SciArt, Corp, which has licensed the Pareto technology (for its finite element capabilities), developed in Prof. Suresh's lab, through Wisconsin Alumni Research Foundation.

References

Allaire G, Geoffroy-Donders P, Pantz O (2018) Topology optimization of modulated and oriented periodic microstructures by the homogenization method. Computers & Mathematics with Applications

Bendsoe MP, Guedes JM, Haber RB, Pedersen P, Taylor JE (2008) An analytical model to predict optimal material properties in the context of optimal structural design. J Appl Mech 61(4):930

Bendsoe MP, Sigmund O (2003) Topology Optimization: Theory, Methods, and Applications, 2nd edn. Springer, Berlin

Blok LG, Longana ML, Yu H, Woods BKS (2018) An investigation into 3D printing of fibre reinforced thermoplastic composites. Addit Manuf 22:176–186

Boschetto A, Bottini L (2014) Accuracy prediction in fused deposition modeling. Int J Adv Manuf Technol 73(5-8):913–928

Botelho EC, Figiel MC, Lauke B (2003) Rezende Mechanical behavior of carbon fiber reinforced polyamide composites. Compos Sci Technol 63(13):1843–1855

Brampton CJ, Wu KC, Alicia Kim H (2015) New optimization method for steered fiber composites using the level set method. Struct Multidiscip Optim 52(3):493–505

Brenken B, Barocio E, Favaloro A, Kunc V, Byron Pipes R (2018) Fused filament fabrication of fiber-reinforced polymers: a review. Addit Manuf 21:1–16

Chougrani L, Pernot JP, Véron P, Abed S (2017) Lattice structure lightweight triangulation for additive manufacturing. CAD Computer Aided Design 90:95–104

Dai C, Wang CCL, Wu C, Lefebvre S, Fang G, Liu Y-J (2018) Support-free volume printing by multi-axis motion. ACM Trans Graph (TOG) 37(4):134

Dapogny C, Estevez R, Faure A, Michailidis G (2019) Shape and topology optimization considering anisotropic features induced by additive manufacturing processes. Comput Methods Appl Mech Eng 344:626–665

Das P, Chandran R, Samant R, Anand S (2015) Optimum part build orientation in additive manufacturing for minimizing part errors and support structures. In: Procedia Manufacturing, vol 1. Elsevier, pp 343–354

Deng S, Suresh K (2015) Multi-constrained topology optimization via the topological sensitivity. Struct Multidiscip Optim 51(5):987–1001

Farzadi A, Solati-Hashjin M, Asadi-Eydivand M, Osman NAA (2014) Effect of layer thickness and printing orientation on mechanical properties and dimensional accuracy of 3D printed porous samples for bone tissue engineering. PLOs One 9(9):e108252

Fernandez-Vicente M, Calle W (2016) Santiago ferrandiz, and andres conejero. Effect of infill parameters on tensile mechanical behavior in desktop 3D printing. 3D Printing and Additive Manufacturing 3(3):183–192

Gao T, Zhang WH, Zhu JH, Xu YJ, Bassir DH (2008) Finite elements in analysis and design topology optimization of heat conduction problem involving design-dependent heat load effect. Finite Elem Anal Des 44:805–813

Gersborg-Hansen A, Bendsøe MP, Sigmund O (2006) Topology optimization of heat conduction problems using the finite volume method. Struct Multidiscip Optim 31(4):251–259

Gibson I, Rosen DW, Stucker B (2010) Additive manufacturing technologies: rapid prototyping to direct digital manufacturing. Springer, New York

Gürdal Z, Haftka RT, Hajela P (1999) Design and optimization of laminated composite materials. Wiley, Hoboken

Huang J, Haftka RT (2005) Optimization of fiber orientations near a hole for increased load-carrying capacity of composite laminates. Struct Multidiscip Optim 30(5):335–341

Knoop F, Schoeppner V (2015) Mechanical and thermal properties of fdm parts manufactured with polyamide 12. Solid Freeform Fabrication Symposium, pp 935–948

Li Q, Steven GP, Querin OM, Xie YM (1999) Shape and topology design for heat conduction by evolutionary structural optimization. Int J Heat Mass Transfer 42(17):3361–3371

Liu J, Gaynor AT, Chen S, Kang Z, Suresh K, Takezawa A, Li L, Kato J, Tang J, Wang CCL et al (2018) Current and future trends in topology optimization for additive manufacturing. Struct Multidiscip Optim, pp 1–27

Luo JH, Gea HC (1998) Optimal bead orientation of 3D shell/plate structures. Finite Elem Anal Des 31(1):55–71

Martínez J, Dumas J, Lefebvre S (2016) Procedural voronoi foams for additive manufacturing. ACM Trans Graph 35(4):12

Mirzendehdel AM, Rankouhi B, Suresh K (2018) Strength-based topology optimization for anisotropic parts. Addit Manuf 19:104–113

Mirzendehdel AM, Suresh K (2015) A deflated assembly free approach to large-scale implicit structural dynamics, vol 10

Mohamed OA, Masood SH, Bhowmik JL (2015) Optimization of fused deposition modeling process parameters: a review of current research and future prospects. Adv Manuf 3(1):42–53

Mulholland T, Falke A, Rudolph N (2016) Filled thermoconductive plastics for fused filament fabrication. In: Solid freeform fabrication, Austin, pp 871—883

Sanati Nezhad A, Barazandeh F, Rahimi AR, Vatani M (2010) Pareto-based optimization of part orientation in stereolithography. Proc Inst Mech Eng B J Eng Manuf 224(10):1591–1598

Pedersen P (1989) On optimal orientation of orthotropic materials. Structural Optimization 1(2):101–106

Prajapati H, Ravoori D, Woods RL, Jain A (2018) Measurement of anisotropic thermal conductivity and inter-layer thermal contact resistance in polymer fused deposition modeling (FDM). Addit Manuf 21:84–90

Qian X (2017) Undercut and overhang angle control in topology optimization: a density gradient based integral approach. Int J Numer Methods Eng 111(3):247–272

Raney JR, Compton BG, Mueller J, Ober TJ, Shea K, Lewis JA (2018) Rotational 3D printing of damage-tolerant composites with programmable mechanics. Proc Natl Acad Sci 115(6): 201715157

Sigmund O (2001) A 99 line topology optimization code written in matlab. Struct Multidiscip Optim 21(2):120–127

Sivapuram R, Dunning PD, Alicia Kim H (2016) Simultaneous material and structural optimization by multiscale topology optimization. Struct Multidiscip Optim 54(5):1267–1281

Stegmann J, Lund E (2005) Discrete material optimization of general composite shell structures. Int J Numer Methods Eng 62(14):2009–2027

Steuben JC, Iliopoulos AP, Michopoulos JG (2016) Implicit slicing for functionally tailored additive manufacturing. Comput Aided Des 77:107–119

Suresh K (2010) A 199-line matlab code for pareto-optimal tracing in topology optimization. Struct Multidiscip Optim 42(5):665–679

Svanberg K (1987) The method of moving asymptotes—a new method for structural optimization. Int J Numer Methods Eng 24(2):359–373

Ulu E, Korkmaz E, Yay K, Ozdoganlar OB, Kara LB (2015) Enhancing the structural performance of additively manufactured objects through build orientation optimization. J Mech Des 137(11):111410–1–111410–9

Umetani N, Schmidt R (2013) Cross-sectional structural analysis for 3D printing optimization. In: SIGGRAPH Asia 2013 Technical Briefs on - SA '13. ACM Press, New York, pp pp 1–4

Walker M, Smith R (2003) A methodology to design fibre reinforced laminated composite structures for maximum strength. Composites Part B 34(2):209–214

Wang MY, Wang X, Guo D (2003) A level set method for structural topology optimization. Comput Methods Appl Mech Eng 192(1-2):227–246

Wikipedia Contributors (2018) Fused filament fabrication — Wikipedia, the free encyclopedia. [Online; accessed 25-May-2018]

Jun W, Clausen A, Sigmund O (2017) Minimum compliance topology optimization of shell–infill composites for additive manufacturing. Comput Methods Appl Mech Eng 326:358–375

Jun W, Wang CCL, Zhang X, Westermann R (2016) Self-supporting rhombic infill structures for additive manufacturing. Comput Aided Des 80:32–42

Xie YM, Steven GP (1993) A simple evolutionary procedure for structural optimization. Comput Struct 49(5):885–896

Yi MX, Zuo ZH, Huang X, Rong JH (2012) Convergence of topological patterns of optimal periodic structures under multiple scales. Struct Multidiscip Optim 46(1):41–50

Yadav P, Suresh K (2013) Assembly-free large-scale modal analysis on the graphics-programmable unit. J Comput Inf Sci Eng 13(1):011003

Yadav P, Suresh K (2014) Large scale finite element analysis via assembly-free deflated conjugate gradient. J Comput Inf Sci Eng 14(4):041008

Yan J, Guo X, Cheng G (2016) Multi-scale concurrent material and structural design under mechanical and thermal loads. Comput Mech 57(3):437–446

Zhang P, Liu J, To AC (2017) Role of anisotropic properties on topology optimization of additive manufactured load bearing structures. Scr Mater 135:148–152

Zhang X, Le X, Panotopoulou A, Whiting E, Wang CCL (2015) Perceptual models of preference in 3d printing direction. ACM Trans Graph (TOG) 34(6):215